Detection of lipid raft domains in neutral and anionic Langmuir monolayers and bilayers of complex lipid composition

Florian Evers,[‡,§] Christoph Jeworrek,[†] Katrin Weise,[†] Metin Tolan,[‡] and Roland Winter [†,*]

† Physical Chemistry I, Faculty of Chemistry, TU Dortmund University, Dortmund, Otto-Hahn-Str. 6, D-44221 Dortmund, Germany

‡ Faculty of Physics and DELTA, TU Dortmund University, Maria-Goeppert-Mayer-Str. 2, D-44221 Dortmund, Germany

§ present address: Condensed Matter Physics Laboratory, Heinrich-Heine-Universität Düsseldorf, Universitätstraße 1, D-40225 Düsseldorf, Germany

* Corresponding author: roland.winter@tu-dortmund.de.

– Supporting Information –

1. X-ray reflectivity and grazing incidence X-ray diffraction measurements

The X-ray scattering experiments were conducted at the liquid surface diffractometer of beamline ID10B at the synchrotron light source ESRF (European Synchrotron Radiation Facility, Grenoble, France).[1] A monochromatic X-ray wavelength, λ, of 1.523 Å or 1.555 Å (corresponding to photon energies, E, of 8.14 keV and 7.97 keV, respectively) was selected by a diamond(111) crystal. The monochromatic beam was deflected to an incident angle, α_i, onto the liquid surface.

Reflectivity scans were carried out by measuring the scattered intensity as a function of α_i under the specular condition $\alpha_i = \alpha_f$ (exit angle, α_f) using a 50 mm gas filled, position-sensitive detector. Reflectivity measurements were performed in an angular range of $0.4\ \alpha_c < \alpha_i < 30\ \alpha_c$ with the critical angle of total reflection of the air-water interface, α_c.

In grazing incidence X-ray diffraction (GIXD), the liquid surface was illuminated at a constant angle slightly below the critical angle of the air-water interface, i.e., $0.8\ \alpha_c$. Under this condition, the incident wave is totally reflected, while the refracted wave becomes evanescent, so that a layer of ~ 76 Å beneath the interface is illuminated by X-rays and, thus, high surface sensitivity is reached. The scattered intensity was measured as a function of the angle between the incident and diffracted beam projected onto the horizontal plane, 2θ, using a gas-filled detector (150 x 10 mm²). The detector had a vertical acceptance of $0 < Q_z < 0.8$ Å^{-1} and a horizontal resolution of $\Delta Q_{xy} = 0.0051$ Å^{-1}. In a typical GIXD scan, the detector is moved in 200 steps in an angular range of $19° < 2\theta < 29°$ (corresponding to 1.36 Å$^{-1} < Q_{xy} < 2.07$ Å^{-1}) counting 15 s per step.

2. Reduction and analysis of surface X-ray scattering data

A detailed description of the theory of X-ray reflectometry and grazing incidence X-ray diffraction can be found in the literature. [2-7] Here, we will only give a brief account of the relations needed for the evaluation of the data.

In reflectivity experiments, incident and reflected beams are symmetrically arranged. Therefore, the momentum transfer has only a vertical component, Q_z, which is given by $Q_z = k\ (\sin(\alpha_i) + \sin(\alpha_f)) = (4\pi/\lambda)\ \sin(\alpha_i)$ with the modulus of the wave vector, $k = 2\pi/\lambda$, and wavelength, λ. The reflectivity, R, is given as the ratio of the specularly scattered intensity to the intensity of the incident X-ray beam. From X-ray reflectivity data, the vertical electron density profile (EDP) of the sample can be inferred. The EDP is laterally averaged in the illuminated area over ordered and unordered domains of heterogeneous lipid layers.

Data reduction comprises background correction, normalization and scaling of the data as a function of Q_z. Due to the rapid decrease of the reflectivity with increasing Q_z, reflectivity

data are often plotted as R/R_F versus Q_z, where R_F is the Fresnel reflectivity of an ideally flat interface. Thus, features in the reflectivity curve stemming from monomolecular layers become easily visible. [8-11] In order to retrieve the EDP from the reflectivity data, a model of the vertical structure of the system is proposed from which the reflectivity is calculated by Parratt's recursive method. [12] The proposed EDP is varied in such a way that the mean square variation, χ^2, of the difference between calculated and observed reflectivity curve is minimized. The EDP is described in terms of the effective density model which assures for continuous profiles even if the roughness is not small compared to the layer thickness. [2] In general, the EDP is given as a stack of homogeneous layers each with a distinct electron density, ρ, layer thickness, d, and interfacial roughness, σ, between adjacent layers. Lipid monolayers are often described by a two-layer model accounting for a lipid head and tail region. [10,11]

Ordered films spread at the air-water interface may be described by a large number of 2D-crystalline domains randomly oriented around the surface normal, which can therefore be described as a 2D powder. [5-7] In a GIXD experiment, the momentum transfer has a horizontal and vertical component, Q_{xy} and Q_z. [5-7]

Reduction of the diffraction data comprises background correction, normalization and scaling of the data as a function of momentum transfer. The diffraction data are presented as (i) contour plots, $I(Q_{xy},Q_z)$, (ii) GIXD patterns, $I(Q_{xy})$, obtained by integrating along Q_z, and (iii) Bragg rod profiles, [5-7] $I(Q_z)$, obtained by integrating over the Q_{xy} range of each Bragg peak, which are a measure of the thickness of a crystalline film. The Q_{xy} positions of the Bragg peaks yield the repeat distances, d_{hk}, of the 2D lattice of the acyl chains according to $d_{hk} = 2\pi/Q_{xy}$, which can be indexed by the two Miller indices h, k to yield the 2D unit cell. Thus, the 2D crystal lattice parameters (a, b, γ) can be extracted from the horizontal position of the maxima of the Bragg peaks. [7,13] We can limit the analysis to chain-like molecules with cylindrical symmetry which may pack in three different unit cells, hexagonal ($a = b$, $\gamma = 120°$), distorted hexagonal ($a = b$, $\gamma \neq 120°$), or oblique ($a \neq b$) . [7,13] The lateral 2D crystalline domain length, L_{xy}, can be inferred from the full width at half maximum (FWHM) of the Bragg peak, ΔQ_{xy}, corrected for instrumental resolution, according to the Scherrer equation. [14]

It is important to note that X-ray reflectivity measurements average over the entire surface in the X-ray footprint area, whereas GIXD experiments only probe domains of two-dimensional crystalline order while the rest of the sample contributes to the background signal.

3. XRR fitting parameters of the data shown in Figure 1 (in the manuscript)

Table S1. Fitting parameters retrieved from the analysis of the X-ray reflectivity data of the lipid monolayer films at a surface pressure of 30 mN/m (cf. Figure 1).

(a) anionic lipid monolayer

layer	ρ / ρ_{H2O}	d [Å]	σ [Å]
subphase	1	---	3.6
head	1.254	11.6	3.4
tail	1.036	14.7	4.1

(b) neutral lipid monolayer

layer	ρ / ρ_{H2O}	d [Å]	σ [Å]
subphase	1	---	3.6
"raft"	1.036	11.2	2.8
head	1.258	14.2	3.3
tail	0.991	10.1	3.1

4. Reproducibility and temporal stability of lipid raft monolayers

Figures S1 and S2 show reduced X-ray reflectivity data of independently prepared monolayers as well as of the temporal stability of a single monolayer for both neutral and anionic lipid monolayers. The XRR curves shown in Figures S1 and S2 indicate the high reproducibility and temporal stability of both types of lipid raft monolayer.

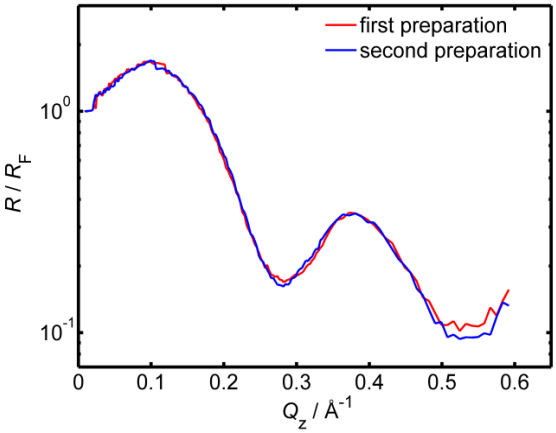

Figure S1. X-ray reflectivity data, normalized to the Fresnel reflectivity, of two independently prepared samples of the neutral lipid monolayer at a surface pressure of 30 mN/m.

a) neutral monolayer

b) anionic monolayer

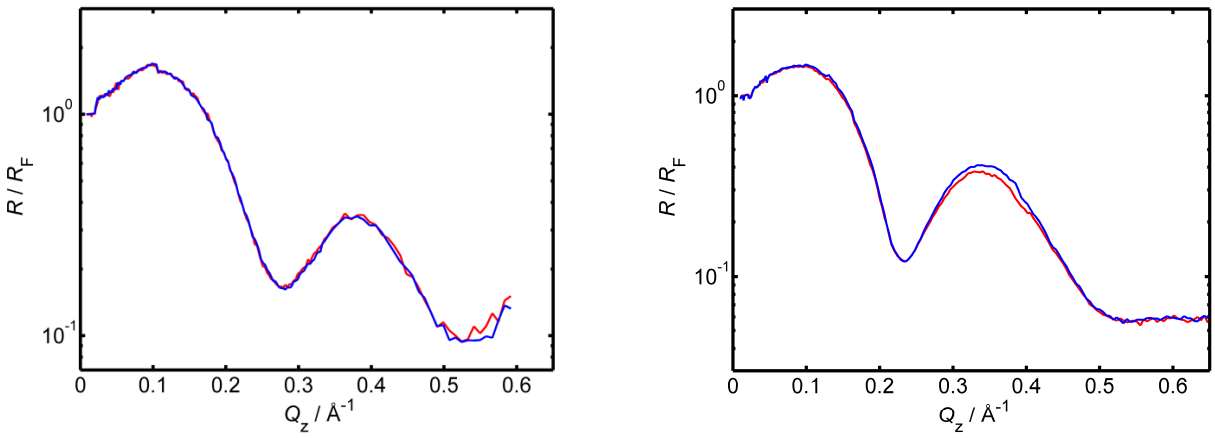

Figure S2. X-ray reflectivity data, normalized to the Fresnel reflectivity, of two consecutive measurements of the same neutral and anionic lipid monolayer at a surface pressure of 30 mN/m.

5. Comparison of various model fits for the neutral lipid monolayer

In Figure S3, different model fits for the neutral lipid monolayer are compared. For this data set, applying the three-layer model reduces the χ^2-value by a factor of about 2.3 compared to the two-layer model. In particular, the minima and maxima of the XRR data are fitted more adequately by the three-layer description. The electron density profiles retrieved from model fitting are displayed as well. For the three-layer model, the electron density of the head group region is slightly increased (as compared to that of the two-layer model), matching the analogous value of the anionic raft monolayer (cf. Table S1).

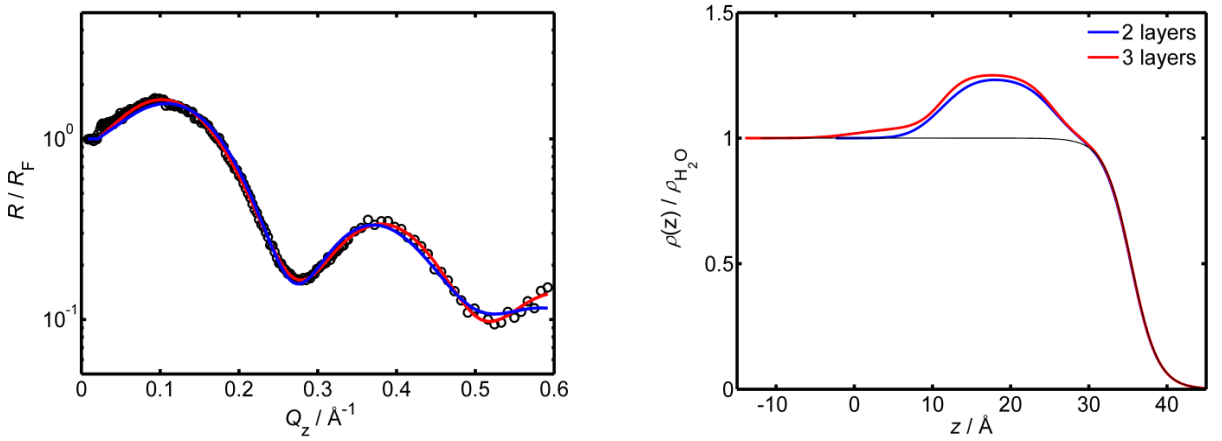

Figure S3. (Left) X-ray reflectivity data (symbols) obtained from neutral lipid raft monolayers at the air-water interface, presented together with the different fitting models (solid lines). (Right) Normalized electron density profiles as retrieved from the fits.

6. Effect of subphase temperature on the vertical structure of anionic lipid raft monolayer films

Figure S4 shows X-ray reflectivity data and electron density profiles of the anionic lipid raft monolayer at two different subphase temperatures. Changing the temperature from 10 °C to 20 °C leads to minor changes in the electron density profile of the monolayer, only. At a temperature of 10 °C, the whole monolayer is slightly thicker, which might be explained by a reduced lateral mobility and an increased order of the lipid tails.

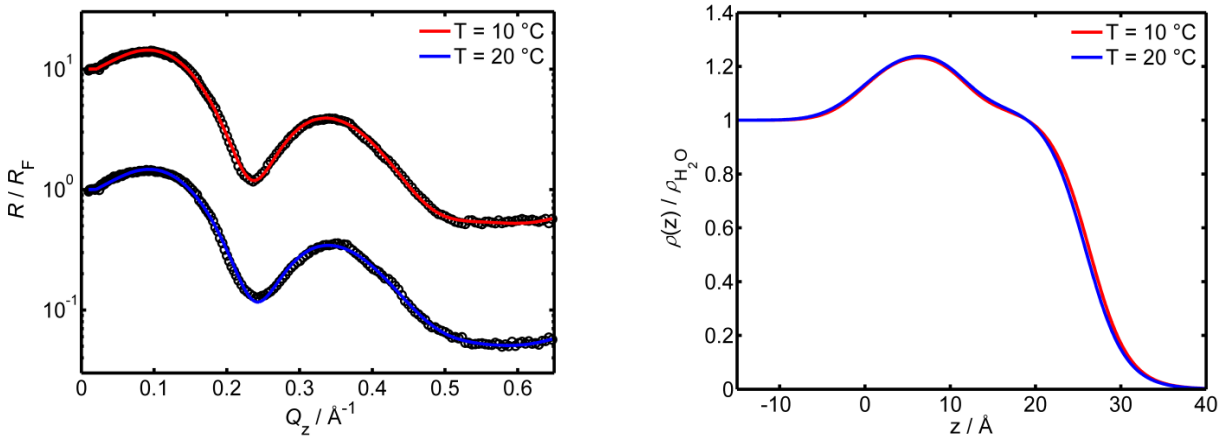

Figure S4. (Left) X-ray reflectivity data (symbols) obtained from anionic lipid raft monolayers at the air-water interface at two different subphase temperatures, presented together with their best fits (solid lines). (Right) Normalized electron density profiles as retrieved from the fits.

7. GIXD measurements of anionic lipid raft monolayer films taken at different film pressures

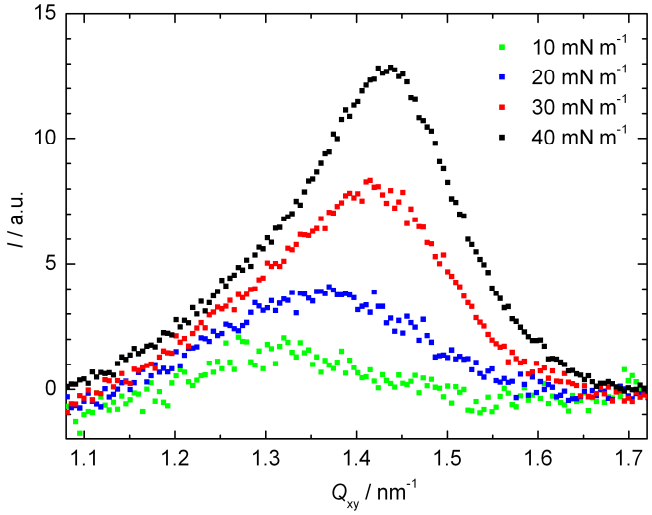

Figure S5. GIXD pattern $I(Q_{xy})$ obtained by integrating along Q_z of an anionic raft lipid monolayer (15% DOPC, 10% DOPG, 40% DPPC, 10% DPPG, and 25% cholesterol, molar ratio) at 20 °C as a function of the film pressure, π. The intensity of the Bragg peaks is not normalised. Measurements were taken – as presented from bottom to top – at π = 10 mN m^{-1} (green), 20 mN m^{-1} (blue), 30 mN m^{-1} (red), and 40 mN m^{-1} (black).

8. GIXD fitting parameters

Table S2. Calculated parameters of grazing incidence diffraction measurements: Lattice vectors in real space, a, b, angle included by lattice vectors, γ, lateral 2D crystalline domain length, L_{xy}, vertical crystalline domain length, L_z, and area per hydrocarbon chain, A_{chain}, are listed for all samples.

	π [mN m^{-1}]	T [°C]	a, b [Å]	γ [°]	L_{xy} [Å]	L_z [Å]	A_{chain} [Å²]
neutral raft	30	10	4.557, 4.568	112.8	100, 386, 1006	17.8, 16.0	19.19
anionic raft	10	20	5.236, 5.236	120.0	18.3	---	25.81
	20	20	5.333, 5.333	120.0	19.9	17.1	24.63
	30	20	5.085, 5.085	120.0	22.2	18.1	22.39
	40	20	5.046, 5.046	120.0	24.1	17.1	22.05
	30	10	5.053, 5.053	120.0	29.9	17.0	22.11
	40	10	5.016, 5.016	120.0	32.0	18.1	21.79

9. Effect of surface pressure on the monolayer structure

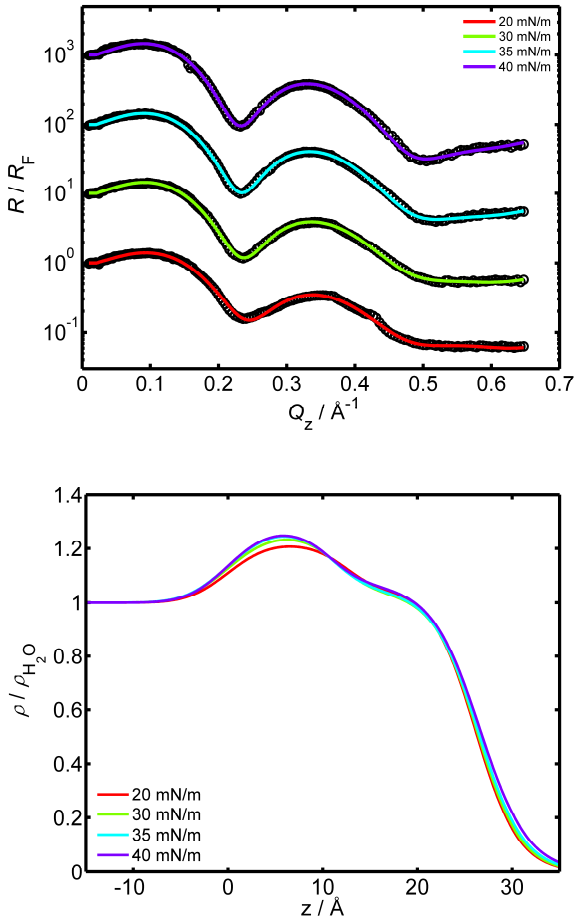

Figure S6. Additional X-ray reflectivity data of the effect of surface pressure on the vertical structure of the anionic lipid monolayer.

References

[1] Smilgies, D.-M.; Boudet, N.; Struth, B.; Konovalov, O. *J. Syn. Radiation* 2005, **12**:329-339.

[2] Tolan, M. X-Ray Scattering from Soft-Matter Thin Films – Materials Science and Basic Research; Springer Tracts in Modern Physics, Berlin, 1999.

[3] Russell, T. P. *Mater. Sci. Rep.* 1990, **5**:171–271.

[4] Daillant, J.; Gibaud, A. 2009. Eds. X-ray and Neutron Reflectivity: Principles and Applications; Lecture Notes in Physics; Springer, Berlin, Heidelberg.

[5] Jensen, T. R.; Kjaer, K. Structural properties and interactions of thin films at the air-liquid interface explored by synchrotron x-ray scattering. In: Möbius, D.; Miller, R. Novel methods to study interfacial layers, Vol. 11. Studies in Interface Science. Amsterdam, Elsevier Science, 2001, pp. 205-254.

[6] Als-Nielsen, J.; Jacquemain, D.; Kjaer, K.; Leveiller, F.; Lahav, M.; Leiserowitz, L. *Phys. Rep.* 1994, **246**:251–313.

[7] Jacquemain, D.; Wolf, S.G.; Leveiller, F.; Deutsch, M.; Kjaer, K.; Als-Nielsen, J.; Lahav, M.; Leiserowitz, L. *Angew. Chem. Int. Ed.* 1992, **31**:130-152.

[8] Paulus, M.; Lietz, D.; Sternemann, C.; Shokuie, K.; Evers, F.; Tolan, M.; Czeslik, C.; Winter, R. *J. Synchr. Radiation* 2008, **15**:600-605.

[9] Hüsecken, A. K.; Evers, F.; Czeslik, C.; Tolan, M. *Langmuir* 2010, **26**:13429–13435.

[10] Evers, F.; Jeworrek, C.; Tiemeyer, S.; Weise, K.; Sellin, D.; Paulus, M. Struth, B.; Tolan, M.; Winter, R. *J. Am. Chem. Soc.* 2009, **131**:9516–9521.
[11] Jeworrek, C.; Evers, F.; Howe, J.; Brandenburg, K.; Tolan, M.; Winter, R. *Biophys. J.* 2011, **100**:2169-2177.
[12] Parratt, L.G. *Phys. Rev.*, 1954, **95**:359–369.
[13] Vineyard, G. H. *Phys. Rev. B* 1982, **26**:4146-4159.
[14] Guinier, A. 1963. X-ray diffraction in Crystals, Imperfect Crystals and Amorphous Bodies; W. H. Freeman: San Francisco.